Distance measurements in nucleic acids using windowless dipolar recoupling solid state NMR

ARTICLE *in* SOLID STATE NUCLEAR MAGNETIC RESONANCE · JANUARY 1997

Impact Factor: 2.27 · DOI: 10.1016/S0926-2040(96)01267-2 · Source: PubMed

7 AUTHORS, INCLUDING:

Myron Hatcher
California State University, Fresno
50 PUBLICATIONS **284** CITATIONS
SEE PROFILE

J. C. Shiels
University of Washington Seattle
4 PUBLICATIONS **294** CITATIONS
SEE PROFILE

ELSEVIER

Solid State Nuclear Magnetic Resonance 7 (1996) 211–228

SOLID STATE
Nuclear Magnetic
Resonance

Distance measurements in nucleic acids using windowless dipolar recoupling solid state NMR

M.A. Mehta [a], D.M. Gregory [b], S. Kiihne [a], D.J. Mitchell [a], M.E. Hatcher [a], J.C. Shiels [a], G.P. Drobny [a,b,*]

[a] *Department of Chemistry, University of Washington, Seattle, Washington 98195, USA*
[b] *Department of Physics, University of Washington, Seattle, Washington 98195, USA*

Received 5 January 1996; accepted 8 April 1996

Abstract

A windowless, homonuclear dipolar recoupling pulse sequence (DRAWS) is described and a theoretical basis for describing its recoupling performance is developed using numerical techniques. It is demonstrated that DRAWS recouples weak dipolar interactions over a broad range of experimental and molecular conditions. We discuss two spectroscopic control experiments, which help to take into account effects due to insufficient proton decoupling, relaxation, and static dipolar couplings to nearby ^{13}C spins at natural abundance. Finally DRAWS is used in combination with selective ^{13}C labeling to measure $^{13}C-^{13}C$ distances in five doubly labeled DNA dodecamers, $[d(CGCGAAT^*T^*CGCG)]_2$, which contain the binding site for the restriction enzyme *Eco*RI. The longest distance reported is 4.8 Å. In most cases the distances agree well with those derived from X-ray crystallographic data, although small changes in hydration level can result in relatively large changes in internuclear distances.

Keywords: Dipolar recoupling; NMR; Nucleic acids

1. Introduction

X-ray crystallography and high resolution multidimensional NMR are presently the principal methods for probing the structures of biopolymers. X-ray crystallography derives the structures of biomolecules from maps of electron density which in turn are calculated from amplitudes and phases of X-rays diffracted from biomolecular crystals [1]. High resolution NMR derives structural information through the interpretation of the Nuclear Overhauser Effect (NOE) observed in systems of coupled protons. Specifically, the average of the inverse sixth power of the internuclear distance $\langle \frac{1}{r^6} \rangle$ is derived from the magnitude of the NOE [2]. Additional structural information is obtained from bond dihedral angles which are calculated from the magnitude of the indirect nuclear–nuclear coupling (also called the *J*-coupling). Although the magnitude of the *J*-coupling constant is not in general related to the bond dihedral angle by any relationship derived from first principles, empirical "rules" have been derived using model compounds which serve to map a cou-

* Corresponding author. Department of Chemistry, Box 351700, University of Washington, Seattle, WA 98195-1700, USA. Tel: (206) 685-0520. fax: (206) 685-8665. e-mail: drobny@macmail.chem.washington.edu.

PII S0926-2040(96)01267-2

pling constant value to a particular geometric configuration of the molecule [3].

Although less frequently utilized than X-ray diffraction and high resolution NMR, solid state NMR has a number of features which recommend it as a complementary structural technique. For instance, like X-ray crystallography, solid state NMR can be applied to crystallized biological polymers. However, solid state NMR can also study biopolymers in mesogenic phases or amorphous solids. In the latter case, the temperature and hydration level of the sample can be systematically varied, enabling the study of biomolecular structure and dynamics over a wide range of physical conditions.

Like high resolution NMR, solid state NMR defines structure by measuring internuclear distances. However, solid state NMR obtains distance information from static dipolar couplings between heteronuclear and homonuclear spins. So unlike high resolution NMR which measures the inverse sixth power of the internuclear distance, it is possible with solid state NMR to obtain the inverse cube of the internuclear distance. This means that all other factors being equal, solid state NMR can measure longer distances than high resolution NMR and thus can contribute distance information that is complementary to data obtained by high resolution NMR. In addition, dihedral angles can be obtained from solid state NMR data, by measuring the mutual orientation between chemical shift anisotropy (CSA) tensors [4–6].

High resolution solid state NMR spectra of rare spin-$\frac{1}{2}$ nuclei are obtained using magic angle spinning (MAS) techniques [7,8] which remove broadening from the CSA. Unfortunately, MAS also attenuates dipolar interactions between homonuclear spin pairs [9]. One of the earliest approaches used to detect homonuclear dipolar interactions under MAS conditions involved matching the sample rotation rate to the difference between the isotropic chemical shifts of the spins [10–14]. This technique, rotational resonance (R^2), has been used to measure internuclear distances in a number of proteins [15,16].

Because R^2 requires matching the rate of sample rotation with the chemical shift difference, it is not practical as a method for detecting a large number of homonuclear dipolar couplings over a broad spectral bandwidth, as would be required in a two dimensional NMR experiment. To accomplish broadband homonuclear dipolar recoupling, the SEDRA [17] and RFDR [18] pulse sequences have been developed. These experiments utilize π-pulses applied within the rotor period to induce a time dependence in the chemical shift difference, which in turn effects a recoupling of homonuclear spins over a broad spectral bandwidth.

Tycko and Dabbagh have recently developed the DRAMA experiment which operates very differently from SEDRA and RFDR. In its simplest version [19], DRAMA consists of a pair of 90° pulses applied during the rotor period. The effect of these pulses is to induce a time dependence of the homonuclear dipolar Hamiltonian in spin space which counteracts the effect of the sample spinning, thus preventing the dipolar interaction from being averaged to zero over a rotor cycle. However, the simple DRAMA experiment does not compensate well for chemical shift anisotropy or offset effects. Recently, a DRAMA super sequence has been introduced by Tycko and Smith [20] which has superior offset/CSA compensation, but dipolar recoupling is not efficiently performed over the entire range of ^{13}C chemical shifts at high magnetic field. An improved DRAMA experiment has also been reported by Klug et al. [21] who call their pulse sequence DRAMAxy8 because trains of phase-shifted π-pulses are applied during a rotor cycle to reduce offset effects.

A dipolar recoupling experiment reported recently by Sun et al. [22] uses rotor-synchronized spin locking to recouple homonuclear dipolar interactions. In this MELODRAMA experiment a finite r.f. field truncates the chemical shift terms in the Hamiltonian when the field strength is appropriately matched to the spinning speed.

Fujiwara et al. [23] have introduced a pulse sequence, later modified by Baldus et al. [24], which achieves efficient zero-quantum polarization transfer using an alternating rotating frame/laboratory frame transfer principle (R/L-driven polarization transfer).

Finally, Spiess and co-workers have recently reported a method for discerning proton–proton connectivities in solids using double-quantum spinning sideband patterns [25].

In a previous paper, we reported distance measurements obtained from model compounds using a windowless, dipolar recoupling pulse sequence, DRAWS (Dipolar Recoupling with A Windowless

Sequence) [26]. Those test compounds were chosen for their range of $^{13}C-^{13}C$ distances and variety of chemical shift tensors. Here, we report the measurement of a number of internuclear distances in selectively ^{13}C-labeled DNA oligomers using DRAWS. We demonstrate the feasibility of using this dipolar recoupling pulse sequence to detect weak dipolar interactions between ^{13}C spins displaying a variety of CSA tensor properties in a biopolymer that has been intensely studied by X-ray crystallography and high resolution NMR.

As a candidate for initial study we chose the palindromic DNA dodecamer $[d(CGCGAATTCGCG)]_2$, which contains the recognition site d(GAATTC) for the restriction enzyme *Eco*RI [27,28]. Although the central portion of the hexamer displays classic B-form structural features, the regions in which the distal nucleotide triplets intersect the ends of the hexamer display sequence-dependent structural modifications which may provide the basis for protein-nucleic acid recognition. For instance, there occurs in the sequence dT8-dC9-dG10 a slip of dC9 away from dT8 and a consequent overlap on dG10. There also occurs a splay in the dC9-dG4 base pair. Both of these structural modifications may contribute to sequence-dependent recognition.

To further investigate the nature and origins of structural modulations in this DNA dodecamer, we have used the DRAWS pulse sequence, in combination with selective ^{13}C labeling to study the structure of this dodecamer as a function of hydration and temperature. We report here our first investigation of the central portion of the restriction enzyme binding site and specifically the structure of the T_7-T_8, site, which is believed to remain relatively unchanged in binding and which deviates little from classic B-form. We also use this DNA oligomer to demonstrate the ability of DRAWS to measure a number of distances between ^{13}C spins characterized by a variety of CSAs.

This paper is organized as follows. In Section 2 we use Average Hamiltonian Theory (AHT) to explain how the pulse sequence DRAWS recouples homonuclear dipolar interactions. Numerical methods will also be used to calculate the effective Hamiltonian under a variety of experimental and molecular conditions. Section 3 describes the preparation of the selectively ^{13}C-labeled DNA dodecamers used in this study. The experimental implementation of DRAWS is also described, and the methods used to obtain numerical simulations of DRAWS experiments are discussed. In Section 4, we present $^{13}C-^{13}C$ distance measurements in five doubly labeled DNA dodecamers at the T_7-T_8 site. In Section 5, we compare the DRAWS distances obtained from the selectively labeled DNA dodecamers with the corresponding distances derived by high resolution solution NMR and X-ray crystallography and discuss the significance of our findings in the broader context of the question of the nature and origins of structural variations in DNA. In Section 6 we discuss directions for future research.

2. Theory and simulations

The basic DRAWS pulse sequence spans one rotor period of length τ_r, and consists of two 90° y-pulses, centered at $\tau_r/4$ and $3\tau_r/4$, with the remainder of the rotor period filled with phase alternated 360° x-pulses. This pulse sequence scheme is shown in Fig. 1. The 90° pulses prevent the dipolar interaction from being averaged to zero, much in the spirit of the DRAMA sequence. The remainder of the r.f. irradiation serves to suppress the chemical shift, with the phase alteration helping to compensate for r.f. inhomogeneity. This basic segment is then supercycled to $R\bar{R}\bar{R}R$, so in a DRAWS experiment, the transverse magnetization is observed stroboscopi-

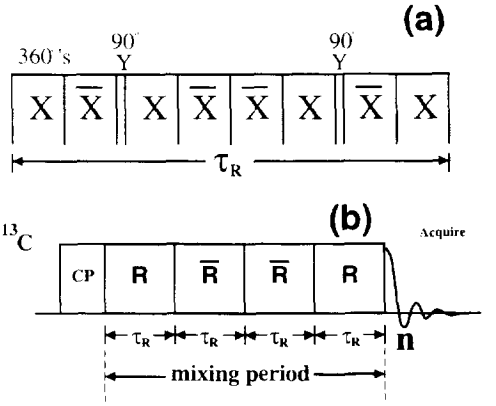

Fig. 1. Dipolar Recoupling using A Windowless Sequence, or DRAWS. The basic sequence over one rotor cycle is shown in 1(a), and the 4-rotor cycle supercycle is given in 1(b).

cally every four rotor cycles. It should be noted that, although the sequence suggests a matching condition between τ_r and $\tau_{r.f.}$ (namely, $\tau_r = 17\tau_{r.f.}/2$) this is not a stringent experimental requirement. DRAWS appears to be relatively impervious to slight variations in the r.f. power, as long as the 90° pulses remain intact. We will support this claim with numerical simulations.

The DRAWS pulse sequence may be described using AHT. Recall that for a system governed by a time-dependent Hamiltonian, $\hat{H}(t)$, the full propagator is given as

$$\hat{U}(t) = T\exp\left(-i\int_O^t dt'\hat{H}(t')\right) \tag{1}$$

where T is the Dyson time ordering operator. Average Hamiltonian Theory [29] uses the Magnus expansion to reconstruct this propagator from a time-independent, Hermitian quantity, $\hat{\bar{H}}$,

$$\hat{U}(t) = \exp(-i\hat{\bar{H}}t),$$
$$= \exp\left[-i\left(\hat{\bar{H}}^{(0)} + \hat{\bar{H}}^{(1)} + \hat{\bar{H}}^{(2)} + \cdots\right)t\right]. \tag{2}$$

The first two terms in the expansion of $\hat{\bar{H}}$ are given by

$$\hat{\bar{H}}^{(0)} = \frac{1}{t}\int_0^t dt'\hat{H}(t') \tag{3}$$

$$\hat{\bar{H}}^{(1)} = \frac{-i}{2t}\int_0^t dt''\int_0^{t''} dt'\left[\hat{H}(t''),\hat{H}(t')\right]. \tag{4}$$

The higher order terms $\hat{\bar{H}}^{(1)}, \hat{\bar{H}}^{(2)}$ etc. arise because the Hamiltonian $\hat{H}(t)$ does not commute with itself at different times.

DRAWS is a windowless sequence, so the r.f. is continually "on". Therefore one must contend with the finite width of the pulses by transforming into a toggling frame [29,30]. This is done by transforming the internal Hamiltonian (chemical shift and dipolar) into the interaction frame of the r.f., as $\hat{H}_{int} = \hat{U}_{r.f.}^{-1}\hat{H}_{int}\hat{U}_{r.f.}$, where

$$\hat{U}_{r.f.}(t) = T\exp\left[-i\int_0^t dt'\hat{H}_{r.f.}(t')\right]. \tag{5}$$

For a pair of dipolar-coupled spins, on resonance and spinning at the magic angle, the DRAWS zeroth order average Hamiltonian has the form

$$\hat{\bar{H}}_D^{(0)} = \frac{d}{17\pi}\left[c_{xx-yy}(I_xS_x - I_yS_y) + c_{zz}\left(3I_zS_z - \vec{I}\cdot\vec{S}\right)\right], \tag{6}$$

where $d = (\hbar\gamma^2)/(r^3)$, and is the static dipolar coupling in radians per second. The coefficients c_{xx-yy} and c_{zz}, which remain after integrating out the time-dependences due to spinning and the r.f., are simply functions of $(\alpha_D, \beta_D, \gamma_D)$, the Euler angles orienting the principal axis of the dipolar tensor in the frame of the rotor. Since the dipolar tensor is uniaxial, α_D is zero. Detailed expressions for c_{xx-yy} and c_{zz} are given in Ref. [6]. We have also shown that, to zeroth order, the DRAWS supercycle completely suppresses the chemical shift terms [26]. Eq. (6) means that unlike a simple MAS experiment where a homonuclear dipolar interaction is averaged to zero to zeroth order [9], DRAWS effects a recoupling of the dipolar interaction and thus a dipolar coupling term appears in the zeroth order average Hamiltonian. This is accomplished while at the same time the chemical shift Hamiltonian is averaged to zero by the end of a supercycle.

We now make use of numerical methods to add to our understanding. It is possible to calculate the average Hamiltonian *to all orders* numerically [31] for a single crystallite orientation. Doing so not only provides a complementary way of investigating the effects of experimental and molecular parameters on dipolar recoupling, but also provides a check for the results derived using AHT. The quantity calculated using the procedure described below is called the effective Hamiltonian, $\hat{H}_{eff}$, which we keep notationally different from Hamiltonians calculated using a Magnus expansion. To calculate $\hat{H}_{eff}$ for DRAWS, we first integrate the equation of motion for the density matrix for a chosen crystallite orientation. Propagators over small time increments are multiplied in a time-ordered fashion, resulting in the numerically exact propagator for the supercycle, $\hat{U}(4\tau_r)$:

$$\hat{U}(4\tau_r) = Te^{-i\int_0^{4\tau_r} dt'\hat{H}(t')},$$
$$= e^{-i\hat{H}(t_N)\delta t_N}\cdots e^{-i\hat{H}(t_2)\delta t_2}e^{-i\hat{H}(t_1)(\delta t_1)}. \tag{7}$$

Next, we solve the equation

$$\hat{U} = e^{-i\hat{H}_{eff}(4\tau_r)} \tag{8}$$

for the *time-independent*, Hermitian quantity, $\hat{H}_{eff}$, by taking the matrix logarithm of the calculated propagator,

$$\hat{H}_{eff} = \frac{i\log(\hat{U})}{4\tau_r}. \tag{9}$$

Given this effective Hamiltonian, which governs the evolution of the spin system under DRAWS, we now seek its operator composition. That is, what is the contribution to $\hat{H}_{eff}$ from the chemical shift terms, or the dipolar terms? In order to determine the component of $\hat{H}_{eff}$ along an operator of interest, we take the trace of $\hat{H}_{eff}$ with that operator. Repeating this procedure for a variety of molecular quantities (CSA values, orientation angles) and experimental parameters (ν_{rf}, ν_r) provides a powerful tool in the development and optimization of a new pulse sequence.

Fig. 2 shows a plot of $\mathrm{Tr}(\hat{H}_{eff} \cdot \hat{H}_{dip})$ as a function of the chemical shift offsets, σ^1_{iso} and σ^2_{iso}, for two ^{13}C spins separated by 2.39 Å. The ^{13}C Larmor frequency is assumed to be 100.54 MHz. The dipolar Hamiltonian is given by

$$\hat{H}_{dip} = \frac{\hbar\gamma^2}{r^3}\frac{3\cos^2\theta - 1}{2}\left(3I_zS_z - \vec{I}\cdot\vec{S}\right), \tag{10}$$

where we have used $\theta = 0$, making the internuclear axis in the crystallite coincident with the laboratory z-axis. We have also scaled the entire surface by the static dipolar coupling, so the surface represents the scaling factor, or the amount of original dipolar coupling recovered. In most molecular settings, the spread of isotropic chemical shifts for ^{13}C spins is usually 200 ppm or less. We can see in Fig. 2 that the dipolar interaction is efficiently recoupled within that bandwidth, and, unlike RFDR and Rotational Resonance, DRAWS works optimally for spins with degenerate chemical shifts. We estimate the optimal dipolar scaling factor at around 0.3, which agrees well with data acquired from model compounds [26]. The surface displayed here is smooth within a region of ± 100 ppm about the resonance, indicating consistent performance across the bandwidth of interest.

It is also interesting to look at the effect of the rotation rate ν_r and the r.f. field strength $\nu_{r.f.}$ on dipolar recoupling. Such a plot is shown in Fig. 3,

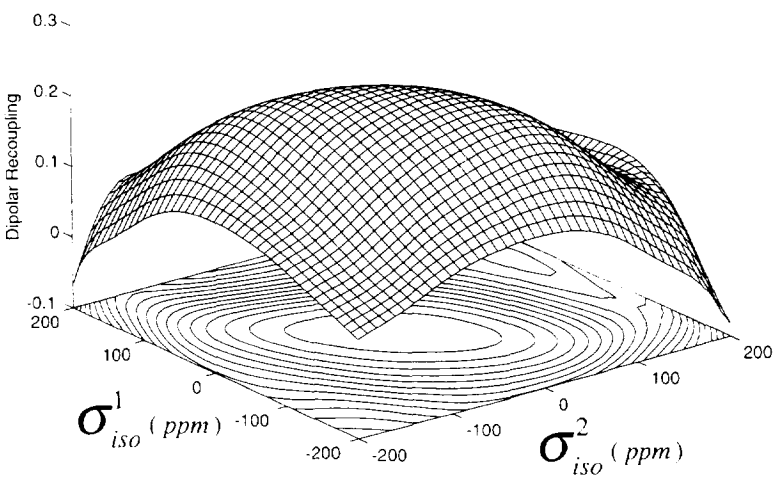

Fig. 2. The dipolar recoupling for DRAWS as a function of offset from resonance for two ^{13}C atoms. $\mathrm{Tr}(\hat{H}_{eff} \cdot \hat{H}_{dip})$ is computed as discussed in the text, for a crystallite with $\theta = 0$. The CSA parameters, in ppm, are those for ^{13}C labeled C_4 and C_6 of 2′-deoxythymidine (C_4: $\delta_{11} = 75.4$, $\delta_{22} = 1.5$, $\delta_{33} = -76.9$; C_6: $\delta_{11} = -93.3$, $\delta_{22} = -7.3$, $\delta_{33} = 100.6$). A realistic ^{13}C–^{13}C distance of 2.39 Å was used, along with a rotor frequency of 5 kHz and an r.f. field strength of 42.5 kHz. The surface is scaled by the static dipolar coupling (3495 rad/s).

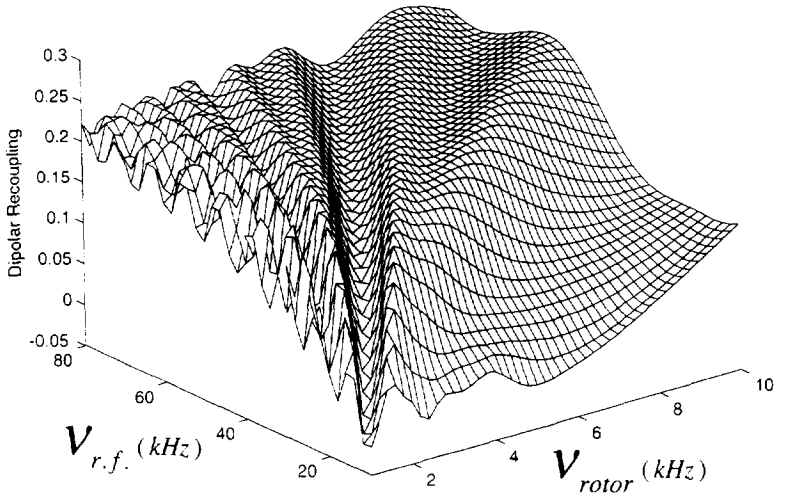

Fig. 3. The dipolar recoupling as a function of the rotor frequency and r.f. field strength. The CSA parameters and internuclear distance are the same as in Fig. 2, however the carrier frequency was set to the center of the two isotropic frequencies (C_4: σ_{iso} = 166.4 ppm, C_6: σ_{iso} = 137.2 ppm).

for the same crystallite orientation as in Fig. 2. As one might expect, DRAWS recouples most efficiently at high rotor speeds and high r.f. field strengths. The ridges in the surface correspond to the various matching conditions, $\tau_r = (8n + 1/2)\tau_{r.f.}$, where the period of the r.f. between the 90° pulses corresponds to an integral number of 360° pulses. Along these ridges the scaling factor is slightly higher. It is clear, though, that at rotor speeds greater than 4 kHz and r.f. field strengths greater than 35 kHz, deviation from the ridges, or the matching conditions, comes at no great cost to recoupling efficiency.

Until now, we have investigated DRAWS by considering time-independent quantities, such as $\hat{H}_D^{(0)}$and $\hat{H}_{eff}$, derived using analytic and numerical procedures. Treating the full time dependence of the problem can also provide additional insights. An especially revealing way to follow the evolution of the system is to track all operator components of the density operator, $\hat{\rho}$, over a supercycle. Practically, this is done by computing the expectation value of each basis operator, $\hat{Q}_i$, by taking its trace with the density matrix, $\mathrm{Tr}(\hat{\rho}(t) \cdot \hat{Q}_i)$. Here, for two coupled spins, we employ a basis consisting of the familiar Cartesian product operators [32] — 15 in all, excluding the identity operator. Fig. 4(a) shows the 15 "lanes" of information for a single crystallite over four rotor cycles, illustrating several important features of the DRAWS sequence. First, the y-magnetization is not spin locked — a favourable circumstance — as spin locking would prevent evolution under the recoupled dipolar Hamiltonian. Second, the initial, y-magnetization is completely transferred to the antiphase modes $(I_x S_z + I_z S_x)$ in one rotor cycle. Third, although multiple quantum coherences (for example, $(I_x S_y + I_y S_x)$) are generated in the course of DRAWS, there is little net production by the end of the supercycle. Finally, the amount of x-magnetization accumulated at the end of a supercycle is small, arising mostly from residual offset terms in the DRAWS Hamiltonian.

In Fig. 4(a), the initial state, $\hat{\rho}(0)$, before the application of DRAWS is the sum of the single-spin transverse magnetizations, $\hat{I}_y + \hat{S}_y$. Fig. 4(b) maps the spin dynamics for $\hat{\rho}(0) = \hat{I}_y - \hat{S}_y$. The lanes in Fig. 4(b) show that, compared with Fig. 4(a), there is no systematic modulation of coherence between the linear modes and the multiple quantum modes or the antiphase modes, so effectively there is no recoupling. In fact, most of the magnetization is confined to the linear modes. We will show in a later section that this effect provides a basis for a control experiment, which can be used to account for decay due to effects other than dipolar recoupling.

Just as we have studied dipolar recoupling effects

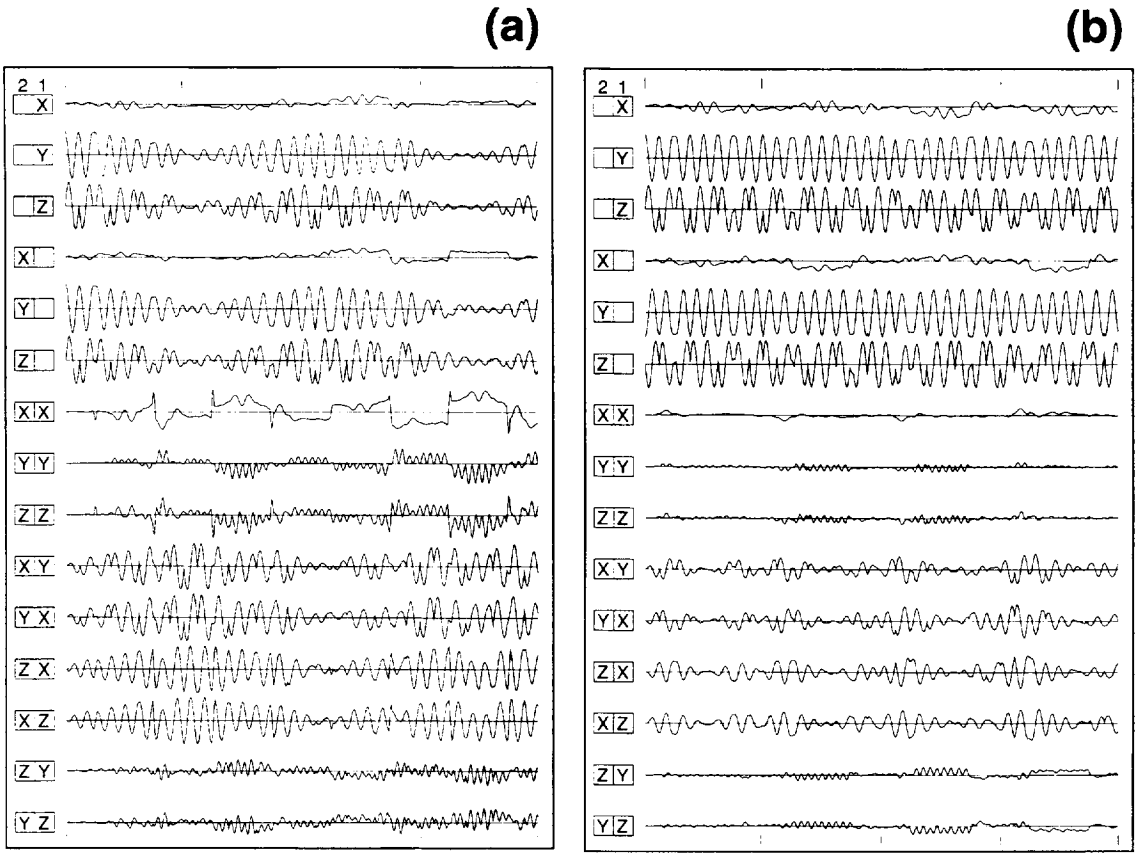

Fig. 4. The spin dynamics, over one supercycle of DRAWS, for a crystallite with the $^{13}C-^{13}C$ internuclear vector initially coincident with the laboratory z-axis. Each lane is computed by evaluating $\mathrm{Tr}(\hat{\rho}(t)\cdot\hat{Q}_i)$, where the $\hat{Q}_i$ are members of the Cartesian product operator basis for two spins. The entry in the "1" column in each tableaux is for the I-spin and in the "2" column for the S-spin. A blank is for the identity operator. For example, a lane labeled as $\overset{2\,1}{XY}$ corresponds to the bilinear operator $\hat{Q}_i = I_y S_x$, whereas $\overset{21}{Z}$ corresponds to the linear operator $\hat{Q}_i = \hat{S}_z$. The CSA parameters are the same as those in Fig. 3. We used $\tau_r = 221$ μs, $\tau_{r.f.} = 26$ μs and a reduced internuclear distance of 1.5 Å. The phases of the pulses for the supercycle are given in Fig. 1. The lanes in 4(a) are for $\hat{\rho}(0) = \hat{I}_y + \hat{S}_y$, whereas those in 4(b) are for $\hat{\rho}(0) = \hat{I}_y - \hat{S}_y$. Tick marks at the top and bottom of 4(a) and 4(b) indicate complete rotor periods.

on individual crystallites, we can simulate experiments on polycrystalline samples by computing powder averages of observables. Within a computational environment, we can easily study the effects of the variation of molecular parameters (CSA values, orientations, distances, etc.) on the final magnetization decay curve. Indeed, in the family of dipolar recoupling experiments discussed in this paper we must do this, because a distance is never discerned directly from an experimental decay curve, but, rather, is inferred from the simulation which best fits the data.

Fig. 5(a) shows a series of simulated decay curves, for a range of $^{13}C-^{13}C$ distances from 2 to 5 Å. The simulations shown here do not include relaxation effects. At short distances, the transverse magnetization decays rapidly, typically oscillating several times before decaying to zero, whereas at longer distances, the signal intensity decays very slowly and monotonically. In principle, the period of oscillation of the signal intensity should provide a measure of the effective dipolar coupling. In actual experiments, however, such oscillations are seen only for short internuclear distances (i.e. less than 3 Å for $^{13}C-^{13}C$ spin pairs), where the coupling is large enough to induce an oscillation in a short amount of mixing time, before magnetization is eventually lost to relax-

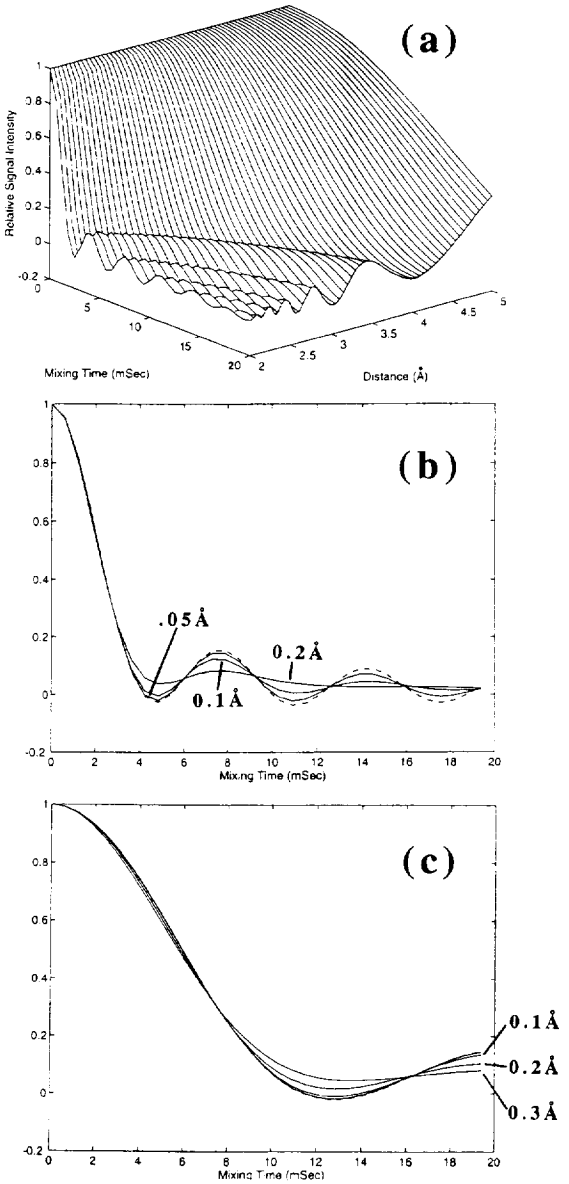

Fig. 5. (a) A stack plot of simulated decay curves for DRAWS over a range of internuclear distances, 2.0 to 5.0 Å, in increments of 0.05 Å. For mixing times of less than 20 ms, dipolar oscillations can be seen below 4.0 Å. Each decay curve is computed using 4000 randomly oriented crystallites, $\tau_r = 153$ μs and $\tau_{r.f.} = 18$ μs. (b) A plot of DRAWS decay curves for an ensemble of isolated spin pairs in which the internuclear distance of the paired spins is 2.5 Å (broken line) and plots of DRAWS decay curves where the internuclear distance of the paired spins varies according to a Gaussian distribution with a mean distance $\bar{r} = 2.5$ Å and standard deviations $\sigma = .05$, 0.1, and 0.2 Å. (c) A plot of DRAWS decay curves for an ensemble of isolated spin pairs in which the internuclear distance of the paired spins is 3.5 Å (broken line) and plots of DRAWS decay curves where the internuclear distance of the paired spins varies according to a Gaussian distribution with a mean distance $\bar{r} = 3.5$ Å and standard deviations $\sigma = 0.1$, 0.2, and 0.3 Å.

ation. This damping also seems to place an upper limit on the range of detectable distances at around 5.0 Å for ^{13}C.

In addition to the magnitude of the internuclear distance, a number of factors can influence DRAWS decay curves. Two important factors are molecular

motions and sample heterogeneity. Molecular motions can average the nuclear dipolar coupling constant either by changing the internuclear distance or by changing the orientation of the internuclear vector. Because biopolymers, and especially nucleic acid polymers, are flexible entities, the presence of such motions must be accounted for in the course of evaluating DRAWS data. Alternatively such motions must be attenuated in some way. In the present study, internal molecular motions are substantially attenuated by performing DRAWS experiments at low temperature, so dynamic averaging of dipolar couplings will not be further discussed here.

However, heterogeneity of molecular environments within a sample may result in a static distribution of internuclear distances and such an effect would not, unlike dynamic averaging, be attenuated at low temperatures. Indeed, static disorder has been observed in DNA and RNA crystals [51,54], so the effect of static disorder should be considered in the evaluation of DRAWS data obtained from DNA in the amorphous solid state.

To account for the effect of a static distribution of structures (i.e. internuclear distances) a form for the distribution must be assumed. We will assume that the internuclear distance between two ^{13}C spins follows a Gaussian distribution. Such a distribution is parametrized by a mean distance $\bar{r}$ and a standard deviation σ. In Fig. 5(b) the DRAWS decay curve is shown for an ensemble of isolated ^{13}C spin pairs, where the paired spins are separated by 2.5 Å (broken line). The series of three solid lines corresponds to DRAWS decay curves for an ensemble of spin pairs where the distances between the paired spins are normally distributed with a mean of $\bar{r} = 2.5$ Å and standard deviations of $\sigma = 0.05$ Å, 0.1 Å, and 0.2 Å. Upon inspection of these curves it is clear that for DRAWS irradiation times of less than 4 ms the curves representing various static distributions of structures deviate little from the ideal distance curve. For times longer than 4 ms, increasing the standard deviation of the distribution damps the DRAWS curve oscillations.

Fig. 5(c) shows that the effect of a static distribution of internuclear distances is even less important for longer distance data. The broken line in the figure corresponds to an ensemble of isolated spin pairs where the distance between the paired spins is 3.5 Å. The three solid lines are DRAWS decay curves for distributions parametrized by a mean of $\bar{r} = 3.5$ Å and standard deviations of $\sigma = 0.1$ Å, 0.2 Å, and 0.3 Å. As before, the static distribution has little effect on the initial slope of the line and damps the long time oscillations.

The simulations in Fig. 5(a) and 5(b), and Fig. 5(c) indicate that although distributions characterized by large dispersions may damp long time oscillations, this is not an effect that would tend to produce errors in distance measurement. Clearly, the effect of increasing distance is to decrease the initial slope of a DRAWS curve. In Section 4 we will show that the minimal changes in initial slope introduced by large structural dispersions (i.e. large standard deviations) generally lie within the experimental error for DNA data. Furthermore, for long distances, damping due to relaxation and incomplete proton decoupling preclude the observation of long time data which would be affected most strongly by structural dispersion. In Section 3 we will describe how damping from relaxation and incomplete decoupling can be accounted for.

Different dipolar recoupling experiments (DRAWS, RFDR, MELODRAMA, Rotational Resonance, etc.) display residual CSA effects to differing extents. This dependence is an issue that merits investigation to achieve a fuller understanding of recoupling, and to fit data for complicated structures where CSA orientations may not be well known. It has been shown, for example, that as the order of Rotational Resonance increases, the dependence on the mutual orientation between CSA tensors grows stronger compared with the dipolar contribution [33]. Similarly, RFDR is known to have a strong orientation dependence at slower spinning speeds for overlapping sideband patterns. Fig. 6(a) and 6(b) show decay curves corresponding to systematic variations in the polar angle between two CSA tensors, at a fixed distance of 4.0 Å, for DRAWS and RFDR. Under comparable experimental conditions, the dependence of DRAWS on the mutual orientation of CSA tensors is clearly much weaker, and it can be made weaker yet by using higher r.f. power. This angular dependence should not be seen as categorically good or bad, but rather something that should be understood and subsequently exploited to one's

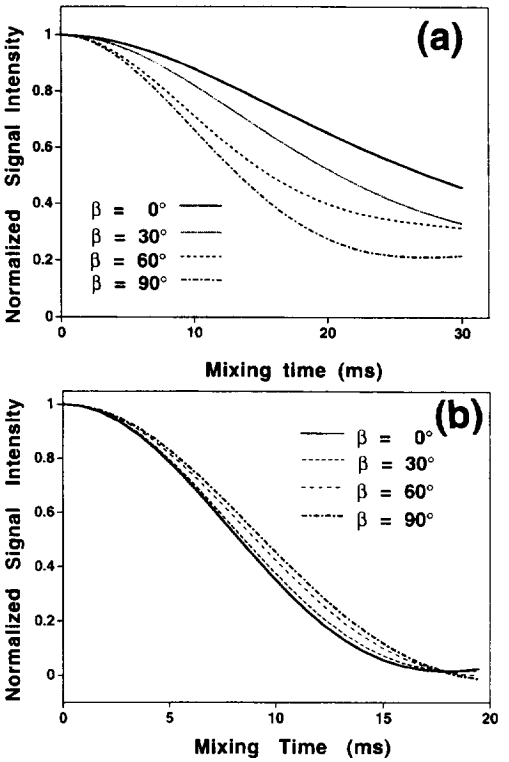

Fig. 6. Dependence of the RFDR (a) and DRAWS (b) decay curves on the polar angle between two CSA tensors under similar experimental conditions. The range of variation is weaker for DRAWS than for RFDR.

advantage. A strong angular dependence in a dipolar recoupling experiment can, in fact, be used to extract additional structural information from the relative orientations of CSA tensors. However, when seeking to measure an internuclear distance, it is desirable to remove this dependence as much as possible, or at least be able to account for its effect.

3. Materials and methods

The ^{13}C labeled DNA samples used in these studies were synthesized on an Applied Biosystems 392 DNA/RNA synthesizer. Phosphoramadites of the ^{13}C labeled thymidine nucleotides were incorporated at the appropriate time to obtain the Dickerson sequence $[d(CGCGAATTCGCG)]_2$ or the DNA hexadecamer $[d(CGAGGTTTAAACCTCG)]_2$. DNA oligomers were purified as described by Alam and Drobny [34]. NaCl was added to each of the DNA samples to make it 10% salt by weight.

Both the $^{13}CH_3$ and $^{13}C'_1$ labeled 2′-deoxythymidines were purchased from Cambridge Isotope Laboratories. The $^{13}C_2$, $^{13}C_4$, and $^{13}C_6$ thymidines, however, were synthesized by the procedures of Redwine and Whaley [35] and Williamson and Boxer [36]. Condensation of the silated base with the 3′,5′-ditoluyl chlorodeoxyribose [37], followed by crystallization and deprotection resulted in the β-anomer of 2′-deoxythymidine. For all the labeled nucleosides, the phosphoramadites were prepared as described by Kintanar et al. [38].

To ensure B-form structures for the DNA dodecamer, samples were brought to high hydration levels by one of two methods. For samples in frozen solution, lyophilized material was dissolved in 50–100 μl of 150 mM phosphate buffer at pH 7.0. For samples with specific water contents, hydration was achieved by allowing the lyophilized material to equilibrate for 3–4 weeks in a closed container with an appropriate saturated salt solution [39]. The extent of hydration was monitored gravimetrically. The DNA hexadecamer was studied as a lyophilized powder.

An important consideration for low temperature studies of nucleic acids is the degree to which freezing perturbs molecular structure. X-ray studies of crystals of $[d(CGCGAATTCGCG)]_2$ at 16 K indicate that the structure of the dodecamer at low temperature is very similar to the structure at room temperature [51,54]. However, freezing a buffered, aqueous solution of DNA may give rise to a number of complications not necessarily encountered in the crystalline samples. Basically, perturbation of molecular structure in a frozen, buffered solution may result from stresses arising from the formation of ice. Formation of ice may result in extremely high solute concentrations because the biopolymer will partition into the non-ice phase. Large pH changes can also occur when buffered solutions are frozen.

Fortunately, the effects of freezing on solutions containing sodium and potassium phosphate salts have been rather thoroughly studied. To summarize, substantial changes in pH and composition occur during freezing in buffered solutions containing sodium and potassium phosphate salts, depending on the initial pH and the relative contents of sodium and

potassium [52,53]. Such studies indicate that for a solution buffered at pH = 7, composition and pH will not be disrupted if the mole ratio of sodium to sodium plus potassium does not exceed 0.85. In all cases presented in this work, this ratio was kept appropriately low to avoid composition and pH variations upon freezing. Cryo-protectants were not used.

NMR experiments were performed on a home-built spectrometer operating at a ^{13}C Larmor frequency of 100.54 MHz. A Chemagnetics variable temperature MAS probe was used with air, speed, and temperature controllers from the same source. All experiments on hydrated DNA dodecamers were performed at -120 ± 2°C, to minimize internal motions, and used dry N_2 for bearing, drive, purge, and temperature control gas. The spin rate was controlled to within ± 10 Hz or less. During cross polarization [40–42]), ^{13}C power levels were 60–62.5 kHz. These levels were lowered to 38.46 or 45.45 kHz during the DRAWS sequence, while ^{1}H decoupling power levels were raised to 110–120 kHz to ensure that no further cross polarization (CP) occurred. Either of two amplifiers, a Kalmus 166HP or a Kalmus LP1000 were used to produce ^{13}C pulses, while a Henry Radio 2004-A linear amplifier was used as the ^{1}H decoupler. A standard tune-up sequence [43] was used to minimize pulse errors.

For the DRAWS measurements, the spin rate was matched to the $\tau_r = 17\tau_{r.f.}/2$ condition to maximize recoupling. Thus, experiments run with a r.f. power level of 38.46 kHz had a spin rate of 4525 Hz, while those at 45.45 kHz used a spin rate of 5348 Hz. The usual 4-rotor period supercycle was expanded to 8 rotor periods, as $R\bar{R}R\bar{R}R\bar{R}R\bar{R}$, to further suppress pulse errors and deviations due to r.f. inhomogeneity.

Each point in a DRAWS decay curve is obtained by integration over all the peaks (i.e. fundamentals and sidebands) in the spectrum of the spin pair. The integrated intensities were normalized to the intensity obtained from a CP/MAS spectrum with no DRAWS applied. In experiments where error estimates are reported, a DRAWS measurement was performed five times, allowing us to estimate the error in the distance measurement. DRAWS was also performed on unlabeled DNA samples in order to measure signal from ^{13}C spins at natural abundance.

Calculations involving the effective Hamiltonian, $\hat{H}_{eff}$, were performed in the MATLAB numerical analysis environment [44]. Simulations of the experimental data were performed on a DEC Alpha workstation using in-house software. The program computes the propagator for a single crystallite over the course of a DRAWS supercycle by assembling propagators over small time increments, and then multiplying the incremental propagators in a time-ordered fashion. Typically, we use time increments of 2–3 μs. The trace of the propagated density matrix with the desired observable, averaged over 4000 randomly oriented crystallites, yields a value which can be compared with the experimental, normalized signal intensity for the same DRAWS mixing time. One crystallite-averaged decay curve takes about 45 min to calculate.

For large molecules and long distances, a control experiment was used to correct for insufficient proton decoupling, dipolar couplings to ^{13}C spins at natural abundance, and relaxation. In cases where sufficient chemical shift resolution exists to prepare the initial state $\hat{I}_y - \hat{S}_y$, the decay curve for this state can be collected, and subsequently simulated with a single phenomenological damping rate. This damping rate is then used in the simulation of the relatively strongly coupled $\hat{I}_y + \hat{S}_y$ state. The TOSS-τ-deTOSS method of Geen et al. was used to prepare the $\hat{\rho}(0) = \hat{I}_y - \hat{S}_y$ state [45].

Unfortunately, the $\hat{I}_y - \hat{S}_y$ state cannot be prepared for species with identical isotropic chemical shifts. To account for relaxation effects and experimental imperfections in these samples, a DRAWS experiment is performed on a singly labeled DNA sample or, if possible, on unlabeled samples. As before, the decay is fit by varying the single quantum damping rate, $(T_2^{SQ})^{-1}$, and this same rate is then used in the simulations of the experiment on the analogous, doubly labeled sample.

Table 1
Chemical shift principal values[a] in ppm

Carbon	σ_{11}	σ_{22}	σ_{33}
C_2	98	124	229
C_4	242	168	90
C_6	44	130	238
C_1'	49	89	121
CH_3	−1.3	−1.3	34.7

[a] $|\sigma_{33} - \sigma_{iso}| \geq |\sigma_{11} - \sigma_{iso}| \geq |\sigma_{22} - \sigma_{iso}|$, values relative to TMS.

Table 2
Euler angles (α, β, γ) in degrees, for transformation from the PAS frame of T_7 and T_8 spins to the dipolar frame in $[d(CGCGAAT^*T^*CGCG)]_2$, and damping constants in milliseconds. The dipolar z-axis points from the T_8 spin to theT_7 spin. All values are derived from an ideal B-form structure. Experimental data on the orientations are determined for the monomer. Orientation within the monomer is assumed to remain unchanged upon incorporation into DNA

T_7-T_8 Spin pair	T_7 Spin → Dipolar	T_8 Spin → Dipolar	T_2^{SQ}	T_2^{DQ}
$^{13}C_2-^{13}C_2$	35, 77, 28	35, 95, 0	20.8	–
$^{13}C_4-^{13}C_4$	24, 30.8, 5	64, 27, 0	20.8	–
$^{13}C_6-^{13}C_4$	8, 52, 162	356, 37, 0	20.8	–
$^{13}C'_1-^{13}C_6$	72, 109, 106	172, 115, 0	12.2	2.2
$^{13}CH_3-^{13}CH_3$	313, 30, 49	55, 73, 315	16.7	16.7

The chemical shift tensor principal values were obtained from CP/MAS experiments using the method of Herzfeld and Berger [46], and in some cases by the analysis of powder patterns. These values are summarized in Table 1. It is assumed that they remain unchanged upon incorporation into the DNA. Orientations of these tensors in a local, molecule-fixed frame were determined experimentally. These orientations, along with an ideal B-form model of DNA, were used to determine the Euler angles used to orient the chemical shift tensors in the common dipolar frame. The angles are given in Table 2.

4. Results

Before discussing carbon–carbon distance measurements between adjacent bases, we describe a control experiment. The purpose of this control experiment is to demonstrate that at low temperatures (i.e. -120°C) motion of the DNA molecule as a whole and localized motions of the 2′-deoxythymidine bases in the DNA dodecamer are reduced to a point that allows measurement of internuclear distance without the necessity of correcting for dynamic averaging of the dipolar coupling. To demonstrate this effect we used DRAWS to measure the distance between the $^{13}C_4$ and $^{13}C_6$ nuclei in 2′-deoxythymidine-4,6-$^{13}C_2$ which had been incorporated into a DNA hexadecamer. In an earlier study we used DRAWS to determine the distance between $^{13}C_4$ and$^{13}C_6$ in a doubly labeled thymidine monomer, 2′-deoxythymidine-4,6-$^{13}C_2$ [26]. As shown in Table 1, the $^{13}C_4$ and $^{13}C_6$ spins both have relatively large chemical shift anisotropies and an isotropic shift difference of about 30 ppm. The DRAWS decay data and best fit simulation for the monomer are shown in Fig. 7(a). A distance of 2.39 Å, derived from X-ray crystallographic data [47], was used in the simulation, along with known CSA principal values and orientations. The DRAWS data obtained from the doubly labeled nucleoside incorporated into the DNA hexadecamer, $[d(CGAGGTTTAAACCTCG)]_2$, at the T_8 position are shown in Fig. 7(b), along with the same simulation as in Fig. 7(a). The data reflect the same $^{13}C_4$ to $^{13}C_6$ distance

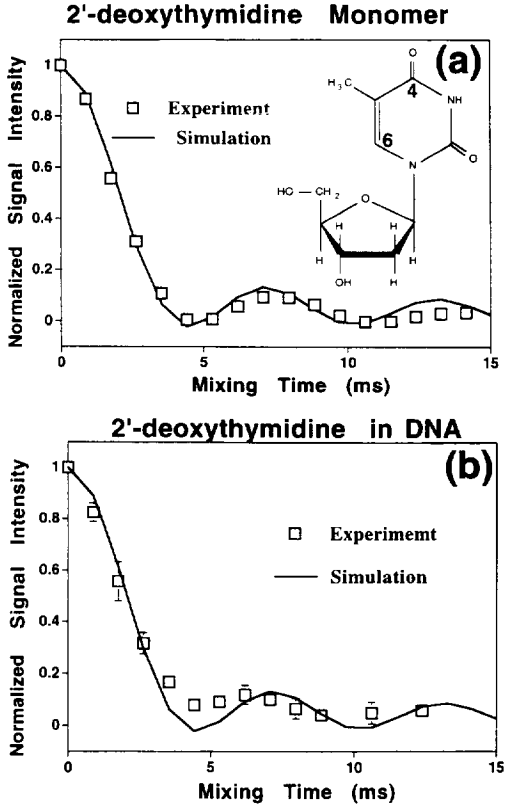

Fig. 7. DRAWS data and simulation for the test experiment. Data for the monomer 2′-deoxythymidine-4,6-$^{13}C_2$ is shown in (a), and the same monomer incorporated into the hexadecamer $[d(CGAGGTTTAAACCTCG)]_2$ in (b). A dipolar oscillation can be seen in the decay curve for the monomer.

in 2′-deoxythymidine before and after incorporation into DNA.

Now we turn our attention to distance measurements between base pairs in the DNA dodecamer. Five doubly ^{13}C-labeled versions of [d(CGCGAATTCGCG)]$_2$ were prepared. As mentioned above the sites of ^{13}C enrichment were located on the T_7 and T_8 2′-deoxythymidines. The pairwise labeling schemes were: C2–C2, C6–C4, C4–C4, C1′–C6, and C5m–C5m (i.e. both methyl carbons labeled). These labeling schemes were chosen for a number of reasons. First, all ^{13}C–^{13}C distances are expected to be over 3.5 Å. Second, the five labeling schemes present an array of CSA tensors and in fact sample virtually all of the ^{13}C CSA scenarios that are encountered in DNA. For example, the C2–C2 and C4–C4 schemes represent coupled carbonyl ^{13}C pairs where the CSA tensors have large anisotropies and virtually identical principal values. The C5m–C5m labeled pair represents a case where the CSA anisotropy is small for both members of the spin pair thus making suppression of the CSA relatively simple. The C1′–C6 labeled pair is perhaps the most challenging case. The members of this spin pair consist of an olefinic carbon (C6) and an alcoholic carbon (C1′). As shown in Table 1 both spins have relatively large chemical shift anisotropies, and there is also a sizeable difference in the isotropic chemical shifts of these spins. In addition both carbon spins are covalently protonated, and unlike the case of the C5m coupled pair, the heteronuclear couplings to the covalently attached protons are virtually unattenuated by motion. Any attempt to measure the C1′–C6 internuclear distance by DRAWS will therefore require very efficient proton decoupling.

In addition to the experimental complications mentioned above, the measurement of ^{13}C–^{13}C distances greater than 3 Å requires a correction for decay due to mechanisms other than the direct dipolar interaction between the members of the spin pair. As discussed in Section 3 for large ^{13}C–^{13}C distances the magnitude of the static dipolar coupling between the ^{13}C spin labels falls to below a few hundred hertz. Under such circumstances dipolar couplings to ^{13}C spins at natural abundance may constitute a competing decay mechanism as may relaxation effects and insufficient proton decoupling. Two of the doubly labeled DNA dodecamers $(^{13}C_{1'})T_7$–$(^{13}C_6)T_8$ and $(^{13}C_6)T_7$–$(^{13}C_4)T_8$, have sufficient isotropic shift resolution to enable preparation of the initial state $\hat{I}_y - \hat{S}_y$. Therefore, in these two cases corrections for competing decay mechanisms were obtained by stroboscopically observing the decay of $\hat{I}_y - \hat{S}_y$ during DRAWS irradiation.

The amplitudes of $\hat{I}_y + \hat{S}_y$ for the $(^{13}C_6)T_7$–$(^{13}C_4)T_8$ doubly labeled DNA dodecamer and for the $(^{13}C_4)T_8$ singly labeled DNA dodecamer, are shown in Fig. 8(A) as functions of the duration of DRAWS irradiation. As mentioned in Section 3 the sample was hydrated to a level of 20 water molecules per nucleotide ($W = 20$) or about 480 waters of hydration per dodecamer. The DRAWS experiment was conducted at -120°C in order to minimize the effects of motional averaging, as discussed above. The control curve was fit to a single exponential decay and yielded a phenomenological T_2 of about 20.8 ms. The experimental $\hat{I}_y + \hat{S}_y$ DRAWS decay curve, corrected using this T_2 value, is displayed along with a family of simulated DRAWS curves for internuclear distances varying from 3.2 Å to 4.2 Å. For mixing times of up to 12 ms the data indicate an internuclear distance of 4.6 ± 0.2 Å.

To probe the effects of hydration on local DNA structure the $(^{13}C_6)T_7$–$(^{13}C_4)T_8$ DNA sample was dissolved in bulk water. The hydration level was gravimetrically determined to be greater than 64 waters per nucleotide or over 1500 waters of hydration per dodecamer. When subsequently cooled to -120°C and subjected to DRAWS irradiation the $(^{13}C_6)T_7$–$(^{13}C_4)T_8$ internuclear distance was found to be 4.0 ± 0.2 Å, as shown in Fig. 8(B). This distance was determined using a control experiment identical to the one described above: a DNA dodecamer singly labeled at the C4 carbon of T_8 was dissolved in bulk water, cooled to -120°C, and subjected to DRAWS irradiation.

A second control study was performed by observing the decay of $\hat{I}_y - \hat{S}_y$ magnetization during DRAWS irradiation from a doubly labeled $(^{13}C_6)T_7$–$(^{13}C_4)T_8$ DNA dodecamer hydrated to $W > 64$ and cooled to -120°C. This second control experiment yielded virtually the same $(^{13}C_6)T_7$–$(^{13}C_4)T_8$ distance, 4.0 ± 0.2 Å. These data are shown in Fig. 8(C).

The 0.6 Å difference in the $(^{13}C_6)T_7$–$(^{13}C_4)T_8$ distance between the two samples equilibrated at

different hydration levels exceeds the experimental error. This result is interesting because at hydration levels of $W = 20$ and $W > 64$, both samples would

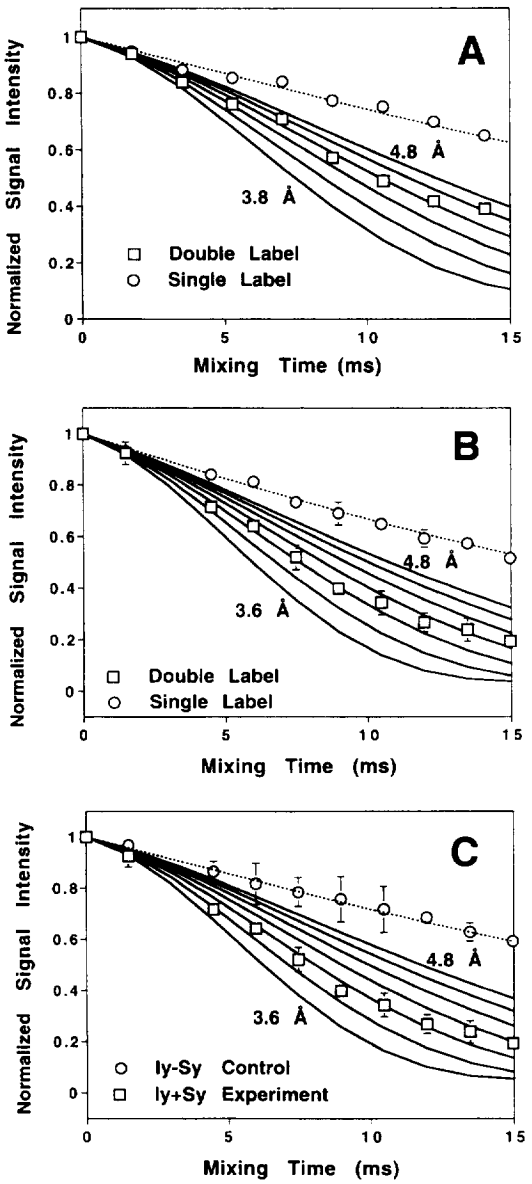

Fig. 8. DRAWS decay curves and simulations for the $(^{13}C_6)T_7$–$(^{13}C_4)T_8$ DNA dodecamer: (A) hydrated to $W = 20$ and evaluated using a singly labeled DNA for a control; (B) the sample hydrated to $W > 64$ and evaluated using a singly labeled DNA dodecamer; (C) the same sample hydrated to $W > 64$ but using the $\hat{I}_y - \hat{S}_y$ control experiment described in the text. In all experiments a t_{90} of 6.5 μs was used.

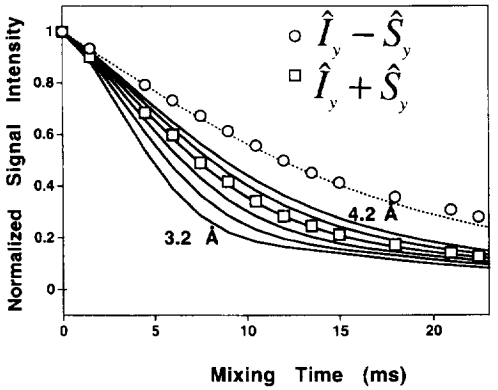

Fig. 9. DRAWS decay curves and simulations for the $(^{13}C'_1)T_7$–$(^{13}C_6)T_8$ DNA dodecamer in frozen solution. Control was provided by the $\hat{I}_y - \hat{S}_y$ initial state. Simulations are plotted (solid lines) in increments of 0.2 Å, from 3.2 to 4.2 Å. A t_{90} of 6.5 μs was used.

be expected to be in the B-form. Thus we observe a significant change in inter-base distance resulting from a transition from the hydrated solid state to levels of hydration similar to solution conditions.

Other labeled DNA dodecamers have not been as thoroughly studied as the $(^{13}C_6)T_7$–$(^{13}C_4)T_8$ sample in the sense that multiple controls were not used and DRAWS data were only obtained at a single hydration level. The $(^{13}C_{1'})T_7$–$(^{13}C_6)T_8$ dodecamer was hydrated to > 43 waters per nucleotide ($W > 43$). As a control, the sample was cooled to -120°C and the decay of the $\hat{I}_y - \hat{S}_y$ observed under DRAWS irradiation. The resulting decay curve (see Fig. 9) was fit to a single exponential and yielded a phenomenological decay constant 12.2 ms. The decay of $\hat{I}_y + \hat{S}_y$ under DRAWS irradiation, corrected using the $\hat{I}_y - \hat{S}_y$ control data, is also shown in Fig. 9 superimposed on a family of simulated DRAWS decay curves ranging from 3.2 to 4.2 Å. For irradiation times up to 14 ms the data are fit best to an internuclear distance of 3.8 ± 0.2 Å.

Three of the five doubly labeled DNA samples contain spin pairs with degenerate chemical shifts, for which the $\hat{I}_y - \hat{S}_y$ control cannot be performed. For the $(^{13}C_2)T_7$–$(^{13}C_2)T_8$ and $(^{13}C_4)T_7$–$(^{13}C_4)T_8$ samples, a DRAWS decay curve was collected using a singly labeled $(^{13}C_4)T_8$ dodecamer. Both C_2 and C_4 are carbonyl carbons with similar chemical shift anisotropies and thus should have similar relaxation

properties when incorporated into the same DNA sequence. The loss of signal intensity in the singly labeled DNA is then taken to be the control, attributed to everything else in the absence of the other carbon in the spin pair, such as residual CSA effects and coupling with the nearby, natural abundance ^{13}C atoms. The decay of $\hat{I}_y + \hat{S}_y$ obtained from the $(^{13}C_4)T_7$–$(^{13}C_4)T_8$ DNA dodecamer under DRAWS irradiation and decay data for the singly labeled $(^{13}C_4)T_8$ dodecamer under similar DRAWS irradiation are shown in Fig. 10. The $\hat{I}_y + \hat{S}_y$ data, corrected for background decay using the singly labeled DNA control data, indicates a $(^{13}C_4)T_7$–$(^{13}C_4)T_8$ internuclear distance of 3.8 ± 0.2 Å. A similar analysis (data not shown) of the $(^{13}C_2)T_7$–$(^{13}C_2)T_8$ DRAWS decay data indicates an internuclear distance of 3.9 ± 0.2 Å.

The third DNA sample with degenerate chemical shifts is the $(^{13}CH_3)T_7$–$(^{13}CH_3)T_8$ dodecamer, bearing labels on the methyl carbons attached to the C_5 carbon of the base ring of the two thymidines. At -120°C, the methyl groups execute fast rotations resulting in small CSAs for the methyl carbons. The $(^{13}CH_3)T_7$–$(^{13}CH_3)T_8$ internuclear distance was determined to be 4.8 ± 0.3 Å for a sample hydrated to $W > 40$.

Best distance estimates derived from DRAWS measurements are summarized in Table 3. These values are compared with distances derived from X-ray crystallographic and solution state NMR studies, and distances from an idealized B-form structure of the DNA dodecamer.

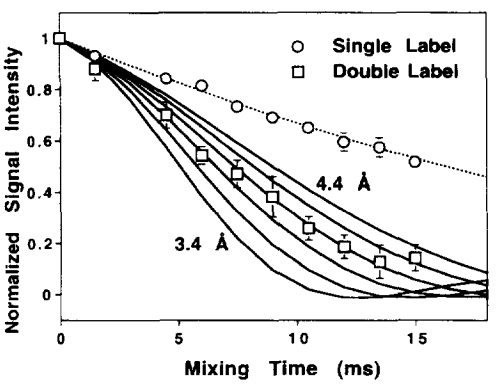

Fig. 10. DRAWS decay curve and simulations for the $(^{13}C_4)T_7$–$(^{13}C_4)T_8$ DNA dodecamer in frozen solution. The control was provided by the singly labeled dodecamer as discussed in the text. A t_{90} of 5.5 μs was used.

Table 3
Internuclear distances for T_7–T_8 in $[d(CGCGAAT^*T^*CGCG)]_2$, in Å

Spin pair	DRAWS	Crystal[a]	Ideal B-form[b]	Solution[c]
$^{13}C_2$–$^{13}C_2$	3.9 ± 0.2	4.07	3.99	3.84
$^{13}C_4$–$^{13}C_4$	3.8 ± 0.2	3.76	3.85	3.36
$^{13}C_6$–$^{13}C_4$ (1)	4.6 ± 0.2	4.45	4.26	4.20
$^{13}C_6$–$^{13}C_4$ (2)	4.0 ± 0.2			
$^{13}C'_1$–$^{13}C_6$	3.8 ± 0.2	4.16	3.59	4.19
$^{13}CH_3$–$^{13}CH_3$	4.8 ± 0.3	4.66	4.75	4.27

[a] Crystal structure values from the work of Dickerson, Drew and co-workers, Ref. [27].
[b] Ideal B-form values measured from an ideal B-form structure using *Insight II*, Version 2.2.0 (Biosym Technologies, San Diego, CA) running on a Silicon Graphics Iris Workstation.
[c] Solution values from the work of Zhu, Ref. [48].
(1) 20 water molecules per nucleotide.
(2) Frozen solution.

5. Discussion

Examination of the data in Table 3 indicates that except for the $^{13}C'_1$–$^{13}C_6$ distance, there is reasonably good agreement between the DRAWS and the X-ray-derived distances. However, a significant result derived from our measurements is the observed variation of inter-base distances in DNA with hydration level. For example, the $(^{13}C_6)T_7$–$(^{13}C_4)T_8$ inter-base distance decreases by 0.6 Å as W increases from 20 to > 60, a range which lies well beyond the putative A- to B-form transition. It is interesting to compare this change with the change in this distance that attends a transition from A- to B-form. Models of ideal A-form and B-form DNA indicate that the $(^{13}C_6)T_7$–$(^{13}C_4)T_8$ distance should change by about 0.5 Å between the two forms. In fact, RFDR dipolar recoupling studies of the $(^{13}C_6)T_7$–$(^{13}C_4)T_8$ labeled DNA dodecamer at very low hydration levels (i.e. $W = 6$), where the DNA is believed to be in the A-form and at higher hydration levels ($W > 10$) where the DNA is believed to be in the B-form, confirm that over this hydration range the $(^{13}C_6)T_7$–$(^{13}C_4)T_8$ distance does decrease by approximately 0.5 Å [49]. These observations seem to indicate that

the change in the $(^{13}C_6)T_7$–$(^{13}C_4)T_8$ inter-base distance that occurs as W approaches 60 is comparable to the change that occurs when the DNA undergoes a transition from A- form to B-form. If this effect occurs for other inter-base distances and for sugar ring conformations, the picture that emerges is that DNA undergoes numerous structural transitions throughout the hydration range $W = 10$–60.

The trend in the change of the $(^{13}C_6)T_7$–$(^{13}C_4)T_8$ inter-base distance as a function of hydration is also interesting. The data in Table 3 indicate that at a lower hydration level of $W = 20$ the $(^{13}C_6)T_7$–$(^{13}C_4)T_8$ inter-base distance of 4.6 Å agrees closely with the X-ray distance of 4.45 Å. However, as W increases to levels comparable to solution conditions, the distance decreases to 4.0 Å, which is closer to the high resolution NMR distances of 4.20 Å. Although the tendency for the DRAWS data to approach the high resolution NMR data as W increases is interesting, there is no reason for the DRAWS-derived distance to agree exactly with the high resolution NMR distance. High resolution NMR data are not corrected for the effects of molecular motions and the DRAWS data were taken under conditions in which these motions should be greatly attenuated.

Finally, the $(^{13}C_6)T_7$–$(^{13}C_4)T_8$ DRAWS data, as well as other data sets, indicate that when damping obtained from experimental controls is applied to DRAWS data, a good match to simulations is generally obtained for mixing times of up to 10 ms. Small deviations for long time data may be the result of structural dispersion, as discussed in Section 2. However, as Fig. 5 indicates, such dispersion does not preclude the accurate measurement of internuclear distances, at least for the normal distribution model considered.

6. Conclusion

In this paper, we have placed DRAWS on a firmer theoretical footing by using numerical calculations to describe the efficiency of dipolar recoupling under a variety of experimental conditions. These conditions include: mutual CSA tensor orientation, frequency offset, spinning speed, and r.f. field strength. We have shown that DRAWS is virtually free of matching conditions that would be indicated by a modulation of recoupling efficiency as a function of the ratio of the r.f. field strength and spinning speed. In fact, at moderate r.f. field strength and at moderate spinning speeds DRAWS recoupling efficiency is not particularly sensitive to r.f. field inhomogeneity or small variations in spinning speed. Furthermore, DRAWS recouples over a broad spectral bandwidth even at moderate spinning speeds and r.f. field strengths, and so is ideally suited to nuclides like ^{13}C which have large variations in isotropic chemical shift. DRAWS also recouples efficiently in the presence of a large chemical shift anisotropy.

In Ref. [26] it was shown that for model compounds ^{13}C–^{13}C internuclear distances of less than 2.5–3.0 Å can be determined to within ± 0.1 Å by direct simulation of DRAWS decay curves. However, for ^{13}C–^{13}C distances greater than 3.0 Å, decay due to effects other than the direct dipolar coupling between the members of the spin pair must be accounted for in the course of evaluating DRAWS data. In this paper, we have described a number of control experiments which are used to derive phenomenological decay constants intended to account for couplings to ^{13}C spins at natural abundance, relaxation, etc.

However, at very long DRAWS irradiation times (i.e. > 12–15 ms for ^{13}C–^{13}C interactions) agreement between simulated DRAWS data and experimental data diminishes in some samples even when corrections derived from control experiments are applied. One explanation for this deviation is neglect of relaxation of double quantum coherence. Fig. 4(a) shows that double quantum coherence is formed in very small amounts after a single DRAWS supercycle. Thus, neglecting the decay of this coherence could therefore conceivably account for poorer agreement between experimental DRAWS data and simulations for long time periods because decay rates derived from control experiments are only applied to single quantum coherence. The only system in which a significant correction was made for decay of double quantum coherence was the $(^{13}C_{1'})T_7$–$(^{13}C_6)T_8$ dodecamer (see Table 3). Had this correction been omitted the agreement of the data to the simulation would have been somewhat poorer for times > 12 ms. For example, the overall effect of omitting the double quantum correction is to diminish the $(^{13}C_6)T_7$–$(^{13}C_4)T_8$ distance by 0.1 Å.

The work presented here points to several avenues for future exploration. First, the effect of hydration level on DNA structure must be further investigated by using DRAWS to measure other internuclear distances over a wide range of W. In addition, DRAWS must be applied to samples of DNA that have been labeled with ^{13}C on the sugar rings and at the 5′ position in order to elucidate the state of the furanose ring pucker and backbone conformation as W changes.

A second direction for future research involves a study of the effect that varying the temperature has on DRAWS measurements. Although all DRAWS experiments in the present study have been carried out at $-120°C$, there is no reason that DRAWS should not be applied to DNA samples at ambient temperature. Such studies would be useful in determining the effect of molecular motions on $\langle 1/r^3 \rangle$. In fact, preliminary data derived from DRAWS studies at ambient temperature indicate that $\langle 1/r^3 \rangle$ for inter-base distances changes significantly [50].

A third direction for future research is the incorporation of DRAWS into multi-dimensional NMR experiments. Obtaining distance information through the preparation and study of pairwise-labeled DNA is straightforward but tedious, time-consuming, and expensive. Preparation of multiply labeled or even uniformly labeled DNA oligomers allows more information to be extracted from a sample but requires the use of two dimensional NMR techniques. DRAWS can be incorporated into the mixing period of a two dimensional pulse sequence and the generalization to higher dimensions is straightforward.

Work in all three directions is in progress.

Acknowledgements

G.P.D. acknowledges support from NIH Program Project Grant GM32681-09. D.M.G. and M.H. acknowledge support from the National Institutes of Health Molecular Biophysics Training Grant GM08268.

References

[1] W. Saenger, Principles of Nucleic Acid Structure, Springer-Verlag, New York, 1984.
[2] R.R. Ernst, G. Bodenhausen and A. Wokaun, Principles of Nuclear Magnetic Resonance in One and Two Dimensions, Oxford University Press, Oxford, 1994.
[3] C.A.G. Haasnoot, F.A.A.M. de Leeuw, H.P.M. de Leeuw and C. Altona, Org. Magn. Reson., 15 (1981) 43.
[4] C.J. Hartzell, T.K. Pratum and G.P. Drobny, J. Chem. Phys., 87 (1987) 4324.
[5] K.W. Zilm and D.M. Grant, J. Am. Chem. Soc., 103 (1981) 2913.
[6] G.S. Harbison, J. Herzfeld and R.G. Griffin, J. Am. Chem. Soc., 103 (1981) 4752.
[7] E.R. Andrew, A. Bradbury and R.G. Eades, Nature, 162 (1959) 1659.
[8] I.J. Lowe, Phys. Rev. Lett., 2 (1959) 285.
[9] M.M. Maricq and J.S. Waugh, J. Chem. Phys., 70 (1979) 3300.
[10] E.R. Andrew, A. Bradbury, R.G. Eades and V.T. Wynn, Phys. Lett., 4 (1963) 99.
[11] M.G. Columbo, B.H. Meier and R.R. Ernst, Chem. Phys. Lett., 146 (1988) 189.
[12] A. Kubo and C.A. McDowell, J. Chem. Soc., Faraday Trans., 84 (1988) 3713.
[13] Z.-H. Gan and D.M. Grant, Mol. Phys., 67 (1989) 1419.
[14] D.P. Raleigh, M.H. Levitt and R.G. Griffin, Chem. Phys. Lett., 146 (1988) 71.
[15] A.E. McDermott, F. Creuzet, R.G. Griffin, L.E. Zawadzke, Q.Z. Ye and C.T. Walsh, Biochemistry, 29 (1990) 5767.
[16] O.B. Peerson and S.O. Smith, Concepts Magn. Reson., 5 (1993) 303.
[17] T. Gullion and S. Vega, Chem. Phys. Lett., 194 (1992) 423.
[18] D.K. Sodickson, M.H. Levitt, S. Vega and R.G. Griffin, J. Chem. Phys., 98 (1993) 6742.
[19] R. Tycko and G. Dabbagh, Chem. Phys. Lett., 173 (1990) 461.
[20] R. Tycko and S.O. Smith, J. Chem. Phys., 98 (1993) 932.
[21] C.A. Klug, W. Zhu, M.E. Merritt and J. Schaefer, J. Magn. Reson., 109 (1994) 134.
[22] B.Q. Sun, P.R. Costa, D. Kocisko, R.T. Lansbury and R.G. Griffin, J. Chem. Phys., 102 (1995) 702.
[23] T. Fujiwara, A. Ramamoorthy, K. Nagayama, K. Hioka and T. Fujito, Chem. Phys. Lett., 212 (1993) 81.
[24] M. Baldus, M. Tomaselli, B.H. Meier and R.R. Ernst, Chem. Phys. Lett., 230 (1994) 329.
[25] J. Gottwald, D.E. Demco, R. Graf and H.W. Speiss, Chem. Phys. Lett., 243 (1995) 314.
[26] D.M. Gregory, D.J. Mitchell, J.A. Stringer, S. Kiihne, J.C. Shiels, J. Callahan, M.A. Mehta and G.P. Drobny, Chem. Phys. Lett., 246 (1995) 654.
[27] R. Wing, H. Drew, T. Takano, C. Broka, S. Tanaka, K. Itakura and R.E. Dickerson, Nature, 287 (1980) 755.
[28] H.R. Drew, R.M. Wing, T. Takano, C. Broka, S. Tanaka, K. Itakura and R.E. Dickerson, Proc. Natl. Acad. Sci. U.S.A., 78 (1981) 217.
[29] M. Mehring, High Resolution NMR in Solids, 2nd Edn., Springer, New York, 1983.
[30] U. Haeberlen, High Resolution NMR in Solids, Selective Averaging, Academic Press, New York, 1976.

[31] H. Liu, S.J. Glaser and G.P. Drobny, J. Chem. Phys., 93 (1990) 7543.
[32] O.W. Sørensen, G.W. Eich, M.H. Levitt, G. Bodenhausen and R.R. Ernst, Prog. NMR Spectrosc., 16 (1983) 163.
[33] D.P. Raleigh, F. Creuzet, S.K. Das Gupta, M.H. Levitt and R.G. Griffin, J. Am. Chem. Soc., 111 (1989) 4502.
[34] T.M. Alam and G.P. Drobny, Biochemistry, 29 (1990) 3421.
[35] C. Redwine and T.W. Whaley, J. Labelled Compd. Radiopharm., 16 (1979) 315.
[36] J.R. Williamson and S.J. Boxer, Nucleic Acids Chem., 16 (1988) 1529.
[37] C.C. Bhat, Synth. Proc. Nucleic Acid Chem., 1 (1968) 512.
[38] A. Kintanar, W.C. Huang, D.C. Schindele, D.E. Wemmer and G.P. Drobny, Biochemistry, 28 (1989) 282.
[39] The Handbook of Chemistry and Physics, 64th Edn., R.C. Weast (Ed.), Chemical Rubber Company, Boca Raton, FL, 1983, p. E-42.
[40] S.R. Hartmann and E.L. Hahn, Phys. Rev., 128 (1962) 2042.
[41] A. Pines, M.G. Gibby and J.S. Waugh, J. Chem. Phys., 59 (1973) 569.
[42] J. Schaefer and E.O. Stejskal, J. Am. Chem. Soc., 100 (1976) 1031.
[43] D.P. Burum, M. Linder and R.R. Ernst, J. Magn. Reson., 43 (1981) 463.
[44] MATLAB, V2.4c, from The MathWorks Inc, 24 Prime Park Way, Natick, MA, 01760.
[45] H. Geen, M.H. Levitt and G. Bodenhausen, Chem. Phys. Lett., 200 (1992) 350.
[46] J. Herzfeld and A.E. Berger, J. Chem. Phys., 73 (1980) 6021.
[47] D.W. Young, P. Tollin and H.R. Wilson, Acta Crystallogr., Sect. B, 25 (1969) 1423.
[48] L. Zhu, Ph.D. Thesis, University of Washington, 1994.
[49] D.M. Gregory, unpublished data, 1995.
[50] S. Kiihne, unpublished data, 1995.
[51] H.R. Drew, S. Samson and R.E. Dickerson, Proc. Natl. Acad. Sci. U.S.A., 79 (1982) 4040-4044.
[52] L. van den Berg, Arch. Biochem. Biophys., 81 (1959) 305-315.
[53] L. van den Berg and D. Rose, Arch. Biochem. Biophys., 81 (1959) 319-329.
[54] S.R. Holbrook and S.H. Kim, J. Mol. Biol., 173 (1984) 361-388.